

# Organic All-Solid-State Lithium Metal Battery Using Polymer/Covalent Organic Framework Electrolyte

Jef Canals,<sup>[a, b]</sup> Boris Irié-Bi,<sup>[b, c]</sup> Franck Dolhem,<sup>[c]</sup> Matthieu Becuwe,<sup>[b, e]</sup> Eric Gautron,<sup>[d]</sup> Vincent Seznec,<sup>\*[b, e]</sup> and Rémi Dedryvère<sup>\*[a, e]</sup>

In this work, we have designed an all-organic and all-solid-state lithium metal battery based on 7,7,8,8-tetracyano-*p*-quinodimethane (TCNQ) as the organic electroactive material and a COF (Covalent Organic Framework)/PEO (PolyEthylene Oxide) composite as solid electrolyte. The use of a solid electrolyte allows fixing the solubility problem of organic electroactive materials in classical liquid electrolytes. This is the first time an all-solid-state organic battery based on TCNQ versus lithium metal is reported, since no liquid additive was included in the formulation of the electrolyte. We obtained a reversible capacity

of 88 mAh g<sup>-1</sup> at the second discharge, and still 58 mAh g<sup>-1</sup> at the tenth discharge. The redox processes were investigated by X-ray Photoelectron Spectroscopy (XPS). We could evidence the involvement of the two lithiation steps of TCNQ (LiTCNQ and Li<sub>2</sub>TCNQ) in the reversible capacity. Optimization of the electrode manufacturing and formulation, and replacing the salt (LiI) by alternative ones opens the door to future improvements in the electrochemical performances. This study demonstrates the interest of COF-type organic structures in the formulation of organic solid electrolytes.

## Introduction

Li-ion batteries (LIBs) are the key technology for portable electronics and electric transportation due to their high energy densities. However, LIBs require inorganic active materials for positive electrodes, which contain transition metals (TMs) that are expensive and raise environmental/ethical issues due the extraction of minerals. Alternatively, organic active materials (OAMs) display high specific capacities due to their low molar masses, and can be synthesized from natural and inexpensive carbonaceous resources.<sup>[1]</sup> Especially, 7,7,8,8-tetracyano-*p*-quinodimethane (TCNQ) is an interesting OAM for positive electrodes due to its ability to reversibly accept two electrons and two Li<sup>+</sup> ions, leading to a high massic capacity (263 mAh g<sup>-1</sup>).<sup>[2-4]</sup> The voltage vs. capacity curve of TCNQ shows two plateaus at 3.0 and 2.7 V vs. Li, corresponding to the obtention of LiTCNQ and Li<sub>2</sub>TCNQ, respectively. Moreover, LiTCNQ can be easily obtained by chemical synthesis.<sup>[5]</sup> However, TCNQ like many OAMs faces a severe solubility issue in organic liquid elec-

lytes, which results in a poor capacity retention upon cycling.<sup>[6-10]</sup> In order to solve this problem, it is possible to use a solid electrolyte in which TCNQ is not soluble, making an all-solid-state battery (ASSB). In a previous paper, Hanyu *et al.*<sup>[2]</sup> have already used this concept to make a quasi-ASSB with TCNQ as active material. The cell was called quasi-ASSB due to the introduction of an ionic liquid in the solid electrolyte. The dissolution of the OAM was prevented by adding a PEO membrane between the electrolyte and the composite organic electrode. With this system, they were able to obtain 100 cycles with a good capacity retention (160 mAh g<sup>-1</sup> at the 90<sup>th</sup> cycle). However, ionic liquids raise themselves safety, price and environmental issues. The aim of the present work is to design a full-ASSB using TCNQ as active material and a composite solid electrolyte based on polyethylene oxide (PEO)<sup>[11]</sup> and a boron-based covalent organic framework (called COF-5).<sup>[12]</sup> We have assessed the electrochemical performances of (Li)TCNQ//PEO-COF-5//Li cells. The redox processes in the cell and the electrode/electrolyte reactivity at solid-solid interfaces have been investigated by X-ray photoelectron spectroscopy (XPS).

[a] J. Canals, R. Dedryvère  
IPREM, CNRS, Université de Pau & Pays Adour, E2S UPPA, 64000 Pau, France  
E-mail: remi.dedryvere@univ-pau.fr

[b] J. Canals, B. Irié-Bi, M. Becuwe, V. Seznec  
LRCS, UMR CNRS 7314, Université de Picardie Jules Verne, 80000 Amiens, France  
E-mail: vincent.seznec@u-picardie.fr

[c] B. Irié-Bi, F. Dolhem  
LG2A, UR 7378, Université de Picardie Jules Verne, 80000 Amiens, France

[d] E. Gautron  
Nantes Université, CNRS, Institut des Matériaux de Nantes Jean Rouxel, IMN, 44300 Nantes, France

[e] M. Becuwe, V. Seznec, R. Dedryvère  
Réseau sur le Stockage Electrochimique de l'Energie (RS2E), FR CNRS 3459, France

 Supporting information for this article is available on the WWW under  
<https://doi.org/10.1002/batt.202400357>

## Experimental Details

### Materials Synthesis

The chemical synthesis of LiTCNQ by reaction of TCNQ with lithium iodide has been performed according to the method described by previous reports<sup>[13,14]</sup>: TCNQ and LiI are dissolved separately in acetonitrile at 60 °C. The whole process is done in argon atmosphere to avoid contamination. The LiI solution is added drop by drop to the TCNQ solution for 12 h. The redox reaction is visually confirmed by the obtention of the dark color of I<sub>2</sub> and a solid product corresponding to LiTCNQ. The product is then filtered, washed with acetonitrile and dried at 100 °C under vacuum.

The Covalent organic framework COF-5 (see Figure 1a) was synthesized<sup>[15,16]</sup> from its commercial precursors, 1,4 diboronic benzene acid (ABDB, sigma-aldrich) and hexahydroxytriphenylene (HHTP, sigma-aldrich). The condensation of these compounds is carried out in a 1:4 volume ratio of dioxane and mesitylene at 90 °C for 5 days under argon with a yield of 69%. Characterization of the obtained COF-5 was performed by high resolution transmission electron microscopy (HRTEM) as displayed in Figure 1b. To this aim, a Thermo Fisher Scientific Themis Z G3 microscope was used. The sample was cooled down to liquid nitrogen temperature, and the electron beam intensity was limited to 1000 e-/Å<sup>2</sup> to prevent from sample degradation. Figure 1b shows the honeycomb structure of COF-5, which is composed of hexagons of 2.7 nm maximal diameter (2.33 nm minimal diameter). Further characterization was performed by Fourier-transform infrared spectroscopy (FTIR), X-ray diffraction (XRD) and selected area electron diffraction (SAED). The results were in good agreement with those reported by other authors<sup>[17]</sup> and are displayed in Figures S1 and S2. Salt impregnation of COF-5 was carried out with lithium iodide (LiI) according to a mass of 0.83 mg of LiI/m<sup>2</sup> of COF. To do so, LiI was dissolved in acetone and the solution was added to the previously degassed dry COF-5 (to remove the adsorbed gases in the pores) kept under

vacuum. The mixture was left under agitation for 7 days at room temperature. After 7 days, the solvent was completely evaporated. The filling of pores by LiI was followed by Brunauer-Emmett-Teller (BET) analysis, showing a decrease of the specific surface area and of pores diameter when the LiI content increases (see Figures S3). The resulting impregnated material will be called COF-5@LiI hereafter. The results in terms of ionic conductivity were investigated by electrochemical impedance spectroscopy, and the Nyquist plots are shown in Figure S4 together with the Arrhenius diagram. The ionic conductivity of the COF-5@LiI studied in this paper is 6.10<sup>-5</sup> S cm<sup>-1</sup> at room temperature (19 °C).

## Electrolyte and Electrode Formulation

### Solid Electrolyte

LiClO<sub>4</sub> salt was dissolved in polyethylene oxide (*i.e.* a mixture of 90 wt.% of 10<sup>5</sup> g/mol PEO and 10 wt.% 5.10<sup>6</sup> g/mol PEO) with a molar ratio of 1 Li<sup>+</sup> for 20 (–CH<sub>2</sub>–CH<sub>2</sub>–O–) units. To do so, 880 mg of PEO mixture and 106 mg of LiClO<sub>4</sub> were dissolved in 2 mL of anhydrous methanol and 5 mL of anhydrous acetonitrile. The

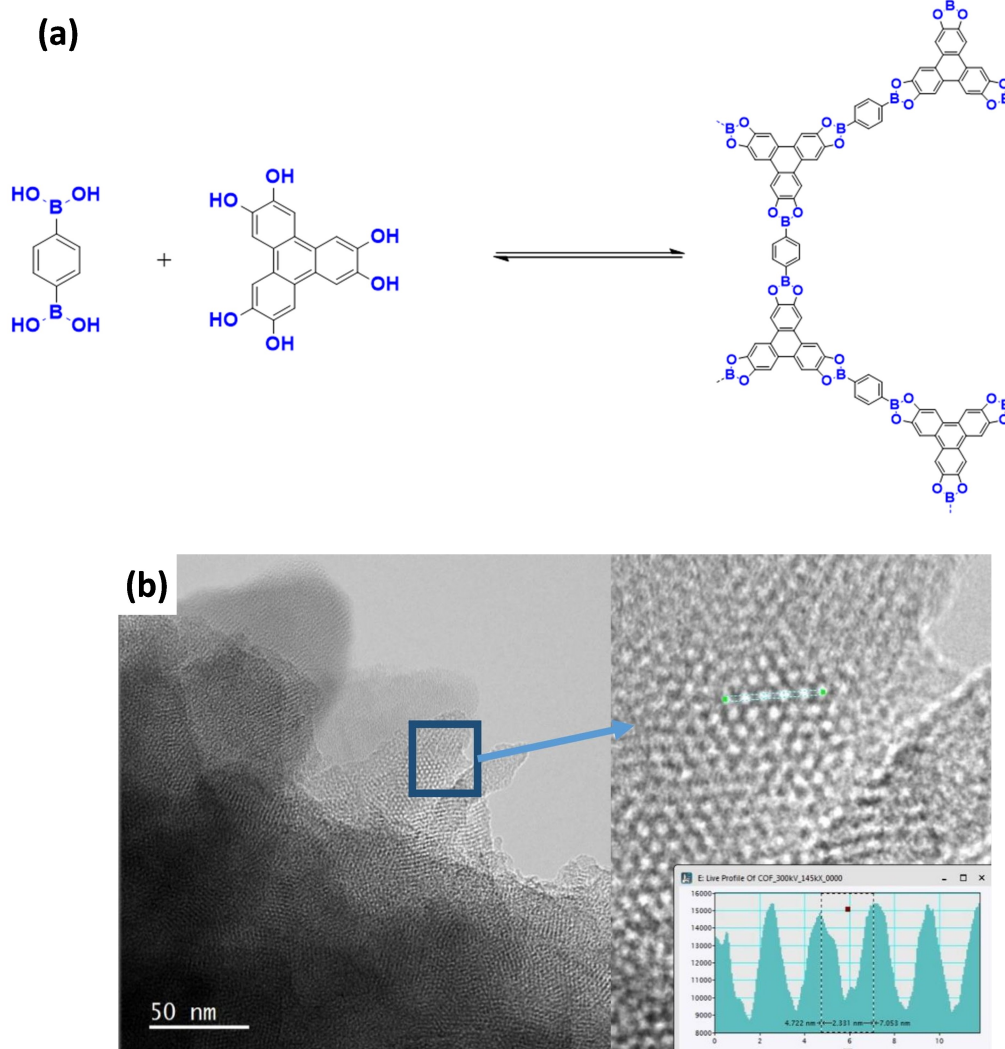


**Figure 1.** (a) Chemical structure of the covalent organic framework COF-5. (b) High resolution transmission electron microscopy (HRTEM) images showing the honeycomb structure of the material.

solution was stirred for several hours, then it was drop-casted onto a clean glass plate (after acetone and isopropanol cleaning) in air in order to cover a 1 dm<sup>2</sup> surface. It was then dried for 24 h, and the obtained electrolyte was stored in an argon glove box after a vacuum drying of 2 h.

### Composite Positive Electrode

In positive electrodes, the OAM is mixed with solid electrolyte and carbon conductive additive in order to ensure good ionic and electronic percolation. The formulation consists in 20 wt.% of LiTCNQ, 70 wt.% of solid electrolyte and 10 wt.% of vapor grown carbon fibers (VGCF).

Two different solid electrolytes were used, either with or without COF-5@Lil. In the COF-free electrolyte, a similar formulation as described above was used. The formulation of the electrolytes containing COF-5@Lil were modified as follows: (i) LiClO<sub>4</sub> salt was replaced by Lil to keep only one salt in the electrode, (ii) The solid electrolyte containing COF5@Lil was obtained by mixing 50 wt.% of Lil-containing PEO and 50 wt.% of COF-5@Lil. The mixtures (880 mg each) were dissolved in 2 mL of anhydrous methanol + 5 mL of anhydrous acetonitrile and stirred for several hours. The slurry was then deposited onto an aluminum current collector by the knife coating technique under argon atmosphere, dried for 2 h in the glovebox, then in vacuum for 2 h. The electrodes were stored under argon.

### Electrochemical Cycling

CR 2032 coin cells in 316 L-stainless steel were assembled in the Ar-filled glovebox, using the composite positive electrode and electrolyte described above, and metallic lithium as the negative electrode.

Electrochemical performances were studied by galvanostatic cycling at C/20 rate at 70 °C, using a biologic VMP3 potentiostat (C/20 means that the positive electrode capacity is reached in 20 h).

### XPS Measurements

XPS characterization was carried out with a ThermoFischer Escalab 250 spectrometer, using a focused monochromatized Al K $\alpha$  source (1487 eV). The samples were handled in a dry argon glovebox directly connected to the XPS introduction chamber in order to avoid any contamination with air and moisture.

To access the buried OAM/solid electrolyte interfaces inside the composite electrode, the current collector and the outermost part of the positive electrode were hand-stripped with a blade under controlled argon atmosphere.

To record the high resolution spectra, a pass energy of 20 eV was chosen. For binding energy (B.E.) calibration, the hydrocarbon C 1s peak at 285 eV was not accessible due to the great signal of VGCF fibers in the composite electrodes. Therefore, the C–O environment of carbon of PEO (C 1s peak at 286.5 eV) was used.

TCNQ was lithiated *in situ* in the XPS ultra-high vacuum chamber by focusing the argon ion gun on a lithium metal target located close to the sample, according to the method previously reported in literature.<sup>[18,19]</sup> The energy of Ar<sup>+</sup> ions was fixed to 2 keV and the spot size to 2 mm.

## Results and Discussion

### Electrochemical Cycling

The choice of chemically lithiated LiTCNQ as electroactive material was made because of its better electronic conductivity compared to non-lithiated TCNQ. Our first attempt was to cycle LiTCNQ in a LiTCNQ-PEO//PEO//Li cell, *i.e.* using the same solid electrolyte formulation in the composite electrode and in the electrolyte compartment. However, we observed almost no reversible electrochemical activity in these conditions, as displayed in Figure 2a. After a first charge up to 3.5 V vs. Li<sup>+</sup>/Li at 70 °C at a C/20 rate, no significant capacity retention was observed during the following discharge and the subsequent cycles.

Therefore, we decided to use a PEO-COF@Lil composite as the solid electrolyte introduced in the composite positive electrode, since COF@Lil was recently evidenced as an interesting solvent-free Li<sup>+</sup> ion conducting material displaying an ionic conductivity of 10<sup>-4</sup> S cm<sup>-1</sup> at room temperature and 10<sup>-2</sup> S cm<sup>-1</sup> at 100 °C.<sup>[20]</sup> In the present paper, we have measured 6.0·10<sup>-5</sup> S cm<sup>-1</sup> at room temperature (19 °C) and 3.6·10<sup>-3</sup> S cm<sup>-1</sup> at 70 °C, which is the temperature of cycling experiments. Such conductivities should be compared to those observed for other kinds of Lil-based composites. Indeed, it is well known that the conductivity of composites obtained from Lil (ionic conductor) and insulators like Al<sub>2</sub>O<sub>3</sub> is significantly increased with respect to pure Lil. One explanation is the role of defects at the insulator-ionic conductor interface, due to the increase in cationic defects concentration at the space-charge region, *i.e.* the region of redistribution of ionic and electronic point defects.<sup>[21–24]</sup> The conductivity of Lil-mesoporous Al<sub>2</sub>O<sub>3</sub> composites was even proven to reach 10<sup>-4</sup> S cm<sup>-1</sup> at room temperature,<sup>[25]</sup> which is more than a thousand times more than pure Lil, and comparable to values obtained for COF-Lil composites. For mesoporous alumina, the increase of conductivity was explained by the decrease of the activation energy for local migration of lithium ions confined within mesopores. Therefore, in our case, we could also explain the good ionic conductivity of the impregnated COF-5@Lil material by the same kind of mechanisms in the mesopores of the COF network.

The LiTCNQ-PEO-COF@Lil//PEO//Li cell was cycled at 70 °C and C/20 rate between 2.7 and 3.15 V vs. Li<sup>+</sup>/Li, as shown in Figure 2b. A much better reversibility was observed, with 0.67 Li<sup>+</sup> inserted per TCNQ unit at the second discharge (~ 88 mAh g<sup>-1</sup>) and still 0.44 Li<sup>+</sup> at the tenth discharge (~ 58 mAh g<sup>-1</sup>). Two discharge processes can be noticed, indicated by horizontal solid lines in Figure 2b: the first one at ~ 2.97–2.98 V and the second one at ~ 2.76–2.77 V (corresponding to ~ 0.4 and ~ 0.3 Li<sup>+</sup> ions inserted at the 2<sup>nd</sup> discharge, respectively). In the charge curves, two reversible steps can be also noticed, indicated by dashed lines: the first one at ~ 3.01–3.02 V, and the second one at ~ 2.86–2.87 V. The latter is a true voltage plateau, at least during the five first cycles. Its potential slightly increases upon cycling (curved dashed line). The observed potentials for these two reversible charge/discharge

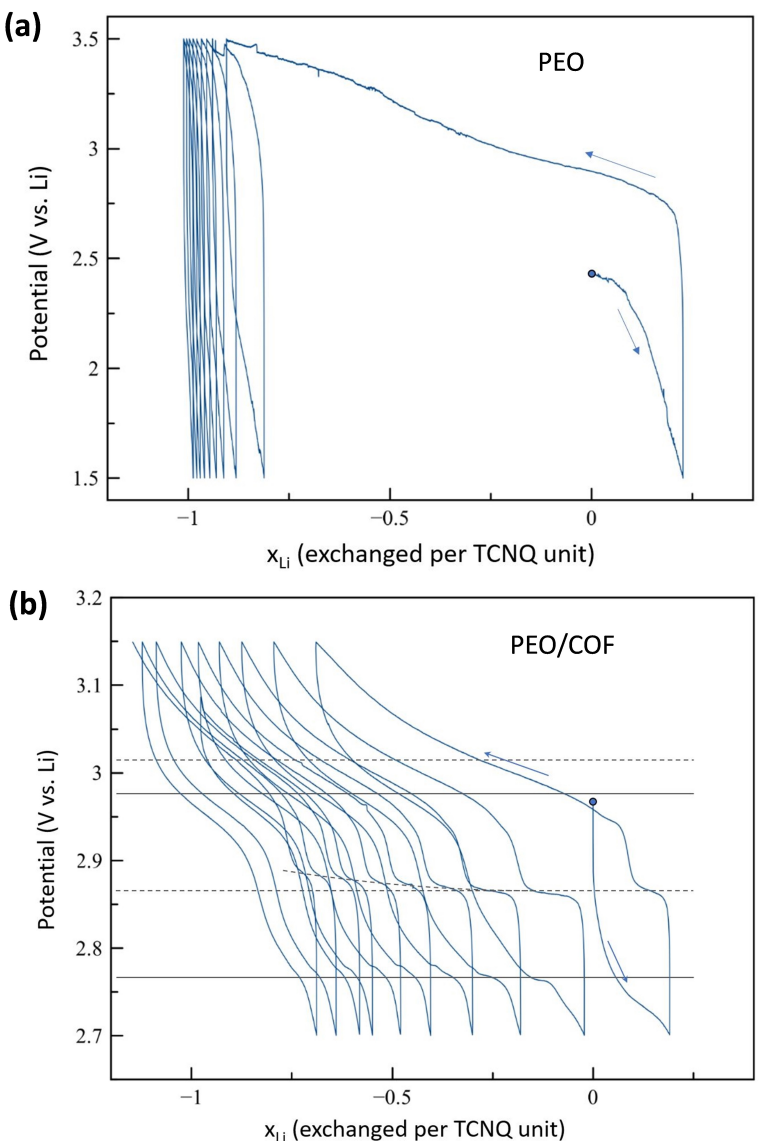


**Figure 2.** Galvanostatic cycling at 70 °C at C/20 rate: (a) LiTCNQ-PEO//PEO//Li cell; (b) LiTCNQ-PEO-COF@Lil//PEO//Li cell.

processes are in good agreement with potentials reported by other authors<sup>[2]</sup> for the first and the second lithiation processes of TCNQ, respectively:  $\text{TCNQ} + \text{Li}^+ + \text{e}^- \rightarrow \text{LiTCNQ}$  and  $\text{LiTCNQ} + \text{Li}^+ + \text{e}^- \rightarrow \text{Li}_2\text{TCNQ}$ . Therefore, the very weak polarization we observe for these two processes (0.04 V and 0.1 V) is a very good result for an all-solid-state cell. This improvement of electrochemical behavior of the battery may be explained by the increased ionic conductivity of the composite polymer electrolyte containing COF@Lil. Different mechanisms can be involved. First, the COF@Lil particles may have the same action as insulating inorganic fillers introduced in a polymer matrix, which increase the amorphousness of the polymer and by the way increase the mobility of polymer chains to promote the diffusion of  $\text{Li}^+$  ions, as it is observed for PEO-Al<sub>2</sub>O<sub>3</sub> composites.<sup>[26–28]</sup> Secondly, the same way as inorganic fillers acting as Lewis acids and creating acid-base interactions with salt anions and oxygen atoms of PEO, and thus leading to

better salt dissociation and mobility of  $\text{Li}^+$  ions,<sup>[29,30]</sup> COF materials show excellent abilities to form Lewis acid-base interactions with salt anions. This ability was evidenced in liquid electrolytes<sup>[31]</sup> and in PEO-based composite solid electrolytes.<sup>[32,33]</sup> Especially, boron-based COFs offer abundant Lewis acidic sites that can promote the dissociation of lithium salts and limit the migration of salt anions by anion-capturing effect, resulting in an increase of the number of freely moving  $\text{Li}^+$  ions, and thus improving the  $\text{Li}^+$  transference number. Finally, our COF@Lil material may also contribute to the conductivity of the composite electrolyte, thanks to its own ion-conducting network through its mesoporous structure.

Going back to Figure 2b, in spite of the very weak polarization, the overall reversibility is still far from the theoretical value of 2 exchanged  $\text{Li}^+$  (263 mAh g<sup>-1</sup>). Moreover, although the redox potential of the  $\text{I}_2/\text{I}^-$  couple is supposed to be outside the voltage window of our cycling conditions (+0.54 V vs. SHE

in aqueous solution corresponds to +3.58 V vs. Li<sup>+</sup>/Li), there is a small risk that LiI participates to the oxidation process occurring at higher voltage (~3 V vs. Li<sup>+</sup>/Li). Therefore, a careful investigation of redox and interfacial processes were performed through XPS analyses.

### XPS Study

#### TCNQ and LiTCNQ

For a better interpretation of changes observed in the shape of XPS spectra, TCNQ was first compared to LiTCNQ obtained by chemical route and to Li<sub>x</sub>TCNQ obtained by *in situ* lithiation in the XPS vacuum chamber. The corresponding N 1s and C 1s XPS spectra are shown in Figure 3. The N 1s spectrum of TCNQ consists in a peak at 399.5 eV (green component) attributed to C≡N functional groups. This peak is accompanied by a π-π\* shake-up satellite (components at 402 and 403 eV), as commonly observed for π-conjugated molecules. Other weak N 1s components may be due to impurities.

The N 1s core peak of LiTCNQ displays a main component at ~398.6 eV, which means a shift of about -1 eV compared to non-lithiated TCNQ. The B.E. position and structure of the N 1s π-π\* satellite is also changed, because the electron delocalization is modified by the addition of an electron in TCNQ<sup>-</sup>. The remaining green component at 399.5 eV is probably due to a

small quantity of TCNQ that did not react with Li. The interpretation of these reference spectra is strengthened by the spectrum of the *in situ* lithiated sample, displaying both N 1s main peaks of TCNQ and LiTCNQ (which also reveals that *in situ* lithiation is incomplete).

The C 1s spectra of TCNQ and LiTCNQ are less resolved since different local environments of carbon are present, labelled 1–4 in the inset of Figure 3. We follow here the interpretation proposed by previous papers<sup>[18,34]</sup> based on the theoretical work of Miller *et al.*<sup>[35]</sup> The C 1s spectrum of TCNQ is dominated by two peaks at 285.2 and 286.7 eV corresponding to C<sub>1</sub> and C<sub>2,4</sub>, respectively. Since the addition of one electron in the system modifies the electron charge distribution, the C 1s spectrum of LiTCNQ is significantly modified, showing three components with the same intensity at 284.5, 285.2 and 286.1 eV attributed to C<sub>1</sub>, C<sub>2,3</sub> and C<sub>4</sub>, respectively. In good agreement with the observation already made on N 1s spectra, the C 1s spectrum obtained after the *in situ* lithiation is a mixture of the two spectra of TCNQ and LiTCNQ with the same area ratio as in N 1s spectrum. Note that the presence of the three weak blue components in the C 1s spectrum of the non-lithiated TCNQ could be explained by the presence of H<sup>+</sup>,TCNQ<sup>-</sup> impurity.<sup>[4,13,35]</sup> Once the characterization of the reference materials has been done, we were able to compare with the data obtained during the redox processes at the OAM/solid electrolyte interface.

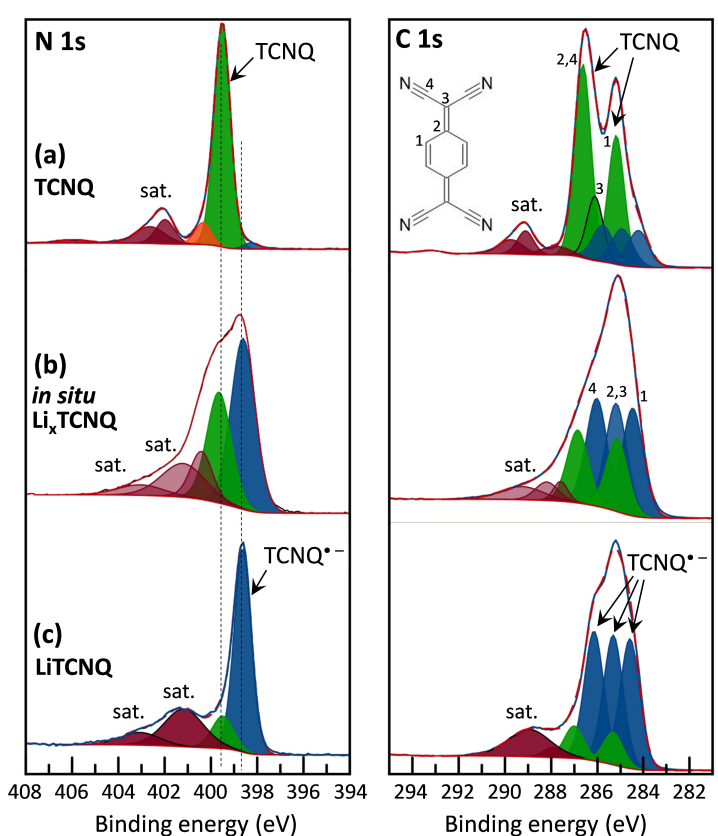


Figure 3. XPS N 1s and C 1s reference spectra of: (a) TCNQ, (b) Li<sub>x</sub>TCNQ (*in situ* lithiation), (c) LiTCNQ (chemically lithiation).

**Redox Processes and Interfaces**

The composite electrode has been manually scraped under inert atmosphere before XPS analysis. This process separates OAM particles from the solid electrolyte to reveal the buried interfaces within the composite electrode. Figure 4 displays the N 1s, C 1s and I 3d XPS spectra of the composite electrode of a LiTCNQ-PEO-COF@LiI//PEO//Li cell, before cycling, after the first discharge, after the following charge (one cycle) and after 10 cycles (10<sup>th</sup> charge), respectively.

The first observation concerns the N 1s spectrum of the pristine electrode (Figure 4a), which clearly displays characteristic peaks of both TCNQ and LiTCNQ in equivalent proportions. This leads us to the conclusion that LiTCNQ has been partly oxidized during the electrode manufacturing process. In parallel, a weak I 3d peak corresponding to I<sub>2</sub> can be detected on the low B.E. side of both I 3d<sub>5/2</sub> and 3d<sub>3/2</sub> components,

besides the main contribution of LiI salt. Traces of I<sub>2</sub> are actually expected due to our synthesis process of LiTCNQ. I<sub>2</sub> is the product of the reduction of TCNQ by LiI (see experimental section). Therefore, the presence of I<sub>2</sub> cannot be responsible for the oxidation of LiTCNQ into TCNQ in the uncycled electrode. This may be due to an interfacial reactivity with the electrolyte before cycling. Besides, the C 1s spectrum of the uncycled electrode is dominated by the characteristic peaks of PEO at 286.5 eV (carbon in one-oxygen environment) and VGCF at 284.5 eV (graphitic-like carbon), as expected.

The N 1s spectrum of the electrode recovered after one discharge (Figure 4b) displays a main peak corresponding to LiTCNQ (dark blue peak at 398.5 eV). A small contribution of TCNQ is still present, while the satellite at ~401 eV (purple) has disappeared and a new peak at lower B.E. is observed (light blue peak at 397–397.5 eV). The electrochemical study of the LiTCNQ-PEO-COF@LiI//PEO//Li cell has shown above that ~0.2

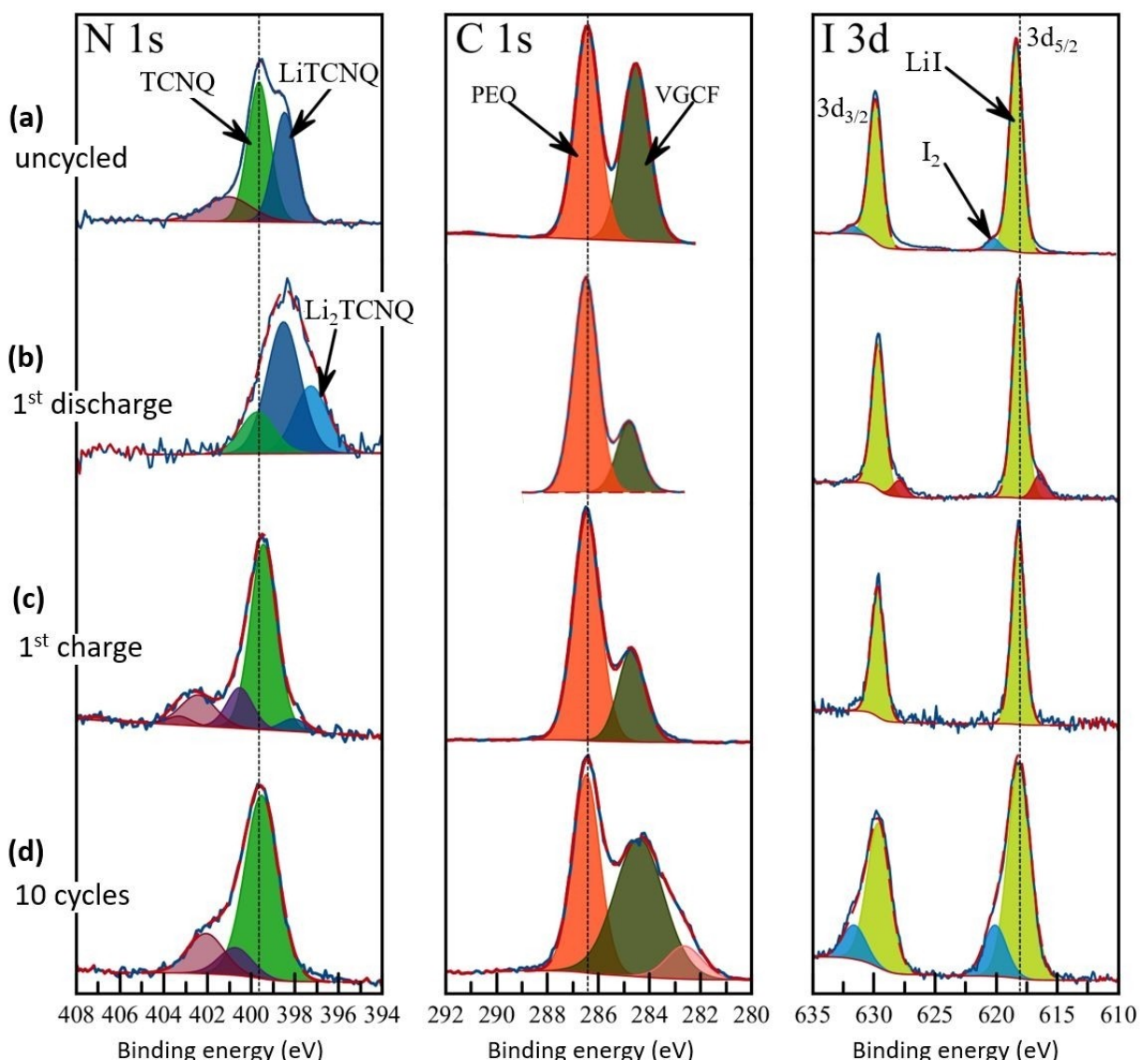


**Figure 4.** N 1s, C 1s and I 3d<sub>5/2-3d<sub>3/2</sub></sub> XPS spectra of the composite positive electrode from a LiTCNQ-PEO-COF@LiI//PEO//Li cell: (a) Uncycled electrode, (b) After one discharge at 1 V vs. Li<sup>+</sup>/Li, (c) After one cycle (first charge), (d) After 10 cycles (10<sup>th</sup> charge).

Li could react with LiTCNQ upon the first discharge. Therefore, we expect that this reaction involves the second lithiation step  $\text{LiTCNQ} \rightarrow \text{Li}_2\text{TCNQ}$ . Note that the sample analyzed in Figure 4b was stopped at 1 V in discharge, which implies a deeper state of discharge compared to the electrochemical curve shown in Figure 2b. The N 1s spectrum after the 1<sup>st</sup> discharge allows to evidence this reduction process, although a small amount of TCNQ is still present (probably some OAM particles are not correctly connected to participate to the reaction). The new N 1s peak at low B.E. is in the range of classical B.E. observed for nitrides. However, in our case it should be assigned to  $\text{Li}_2\text{TCNQ}$ , the low B.E. being explained by the high negative charge on  $\text{TCNQ}^{2-}$ .

Moreover, the disappearance of the N 1s shake-up satellite gives an information on the redox process, because it suggests that the electron delocalization has been significantly modified. Since Miller *et al.*<sup>[35]</sup> have calculated that the electron is mainly transferred to N and C<sub>3</sub> during the second lithiation step, while it is more uniformly distributed to the whole molecule during the first lithiation step, this confirms that the second lithiation step is involved, leading to  $\text{Li}_2\text{TCNQ}$  during the discharge. This is summarized in Figure 5.

Besides, the C 1s spectrum of the discharged electrode shows no significant modification, apart from a change in the PEO to VGCF ratio. The I 3d peak displays a new component at low B.E. (orange). This cannot be explained by a new chemical species, because I<sup>-</sup> is already at the most negative charge in  $\text{LiI}$  due to the high electronegativity difference between Li and I. It would rather be explained by a splitting between the I 3d signal of  $\text{LiI}$  in the composite electrode and in the electrolyte region due to differential charging effect during the XPS experiment. Indeed, the composite is electronically conducting due to the presence of VGCF while the electrolyte region between the two electrodes is electronically insulating, leading to very different behaviors regarding the charge compensation following the departure of photoelectrons from the surface.

The spectra obtained after the 1<sup>st</sup> and the 10<sup>th</sup> charge (*i.e.* at the end of the 1<sup>st</sup> and the 10<sup>th</sup> cycle, respectively) are displayed in Figure 4c and 4d. Note that the samples for analyses after 1 and 10 cycles were cycled between 2.7 and 3.15 V and stopped at 3.15 V. The N 1s spectrum after the 1<sup>st</sup> charge displays an almost complete re-oxidation of the active material into TCNQ,

since its N 1s spectrum is rather close to the TCNQ reference. Only a weak contribution of LiTCNQ still remains detectable. Its I 3d spectrum reveals the sole presence of  $\text{LiI}$ . The N 1s spectrum after the 10<sup>th</sup> charge shows the complete oxidation of TCNQ. However, the overall shape of the spectrum is slightly modified and broadened, without any clear explanation for it. This broadening is also observed on the C 1s spectrum, with a parasitic peak at low B.E. certainly attributed to spectroscopic charging effect (otherwise, it would be attributed to carbides, which is unlikely). Besides, the I 3d spectrum reveals the presence of  $\text{I}_2$  in significant amount, which allows to evidence a progressive formation of  $\text{I}_2$  upon cycling. This is thus the confirmation that iodine slightly participates to the redox reaction, and accumulates upon prolonged cycling. This problem could be easily fixed by the use of an alternative salt in the electrolyte.

## Conclusions

As a conclusion, we have demonstrated the feasibility of an all-solid-state organic lithium metal battery. Our all-solid-state and all-organic system has shown an acceptable cyclability at this first level of research. We have demonstrated the redox activity of the  $\text{Li}_x\text{TCNQ}$  active material upon charge and discharge, without any evidence of degradation of both the active material and the solid electrolyte. A parasitic participation of iodine to the redox processes has been observed, which will be addressed in future work by replacing this salt by another one with increased anodic stability. Optimization of electrode processing and formulation (which has not been done yet) will also provide improvement of the electrochemical behaviour, by improving mechanical contacts between materials, and therefore electronic/ionic percolation, to increase the number of active material particles participating to the redox reaction, and therefore the reversible capacity. Moreover, we have shown the interest of our salt-impregnated COF in the formulation of the solid electrolyte.

It is also important to note the considerable improvement in electrochemical performance between the PEO system alone and the COF/PEO system, showing the contribution of COF in

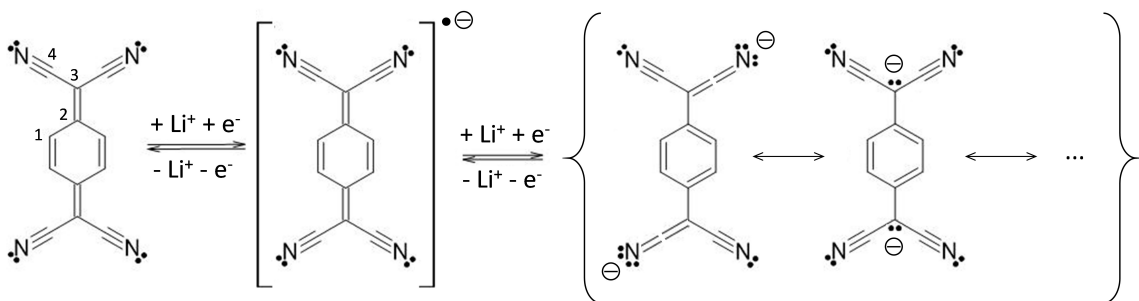


Figure 5. Lithiation mechanisms in TCNQ.

terms of ionic conductivity and the physical integrity of the electrode.

## Acknowledgements

All authors acknowledge the French National Research Agency (ANR) for its support through the Labex STORE-EX project (ANR-10LABX-76-01) and through the DEOSS project (ANR-18-CE05-0018). HRTEM measurements were performed using IMN's characterization platform, PLASSMAT, Nantes, France.

## Conflict of Interests

The authors declare no conflict of interest.

## Data Availability Statement

The data that support the findings of this study are available from the corresponding author upon reasonable request.

**Keywords:** Lithium batteries · organic batteries · XPS · Covalent Organic Framework · TCNQ · polymer electrolyte · polyethylene oxide

- [1] Y. Lu, Q. Zhang, L. Li, Z. Niu, J. Chen, *Chem* **2018**, 4(12), 2786–2813, <https://doi.org/10.1016/j.chempr.2018.09.005>.
- [2] Y. Hanyu, I. Honma, *Sci. Rep.* **2012**, 2(1), 453, <https://doi.org/10.1038/srep00453>.
- [3] C. Fang, Y. Huang, L. Yuan, Y. Liu, W. Chen, Y. Huang, K. Chen, J. Han, Q. Liu, Y. Huang, *Angew. Chem. Int. Ed.* **2017**, 56(24), 6793–6797, <https://doi.org/10.1002/anie.201701213>.
- [4] K. El Kacemi, M. Lamache, *Electrochim. Acta* **1986**, 31(7), 845–849, [https://doi.org/10.1016/0013-4686\(86\)85016-2](https://doi.org/10.1016/0013-4686(86)85016-2).
- [5] M. J. Capitán, J. Alvarez, F. Yndurain, *Phys. Chem. Chem. Phys.* **2018**, 20(33), 21705–21715, <https://doi.org/10.1039/C8CP02438C>.
- [6] S. Zhang, S. Ren, D. Han, M. Xiao, S. Wang, L. Sun, Y. Meng, *ACS Appl. Mater. Interfaces* **2020**, 12(32), 36237–36246, <https://doi.org/10.1021/acsami.0c11241>.
- [7] Q. Deng, Z. Luo, R. Yang, J. Li, *ACS Sustain. Chem. Eng.* **2020**, 8(41), 15445–15465, <https://doi.org/10.1021/acssuschemeng.0c05884>.
- [8] J. J. Shea, C. Luo, *ACS Appl. Mater. Interfaces* **2020**, 12(5), 5361–5380, <https://doi.org/10.1021/acsami.9b20384>.
- [9] E. J. Son, J. H. Kim, K. Kim, C. B. Park, *J. Mater. Chem. A* **2016**, 4(29), 11179–11202, <https://doi.org/10.1039/C6TA03123D>.
- [10] Y. Wu, R. Zeng, J. Nan, D. Shu, Y. Qiu, S. Chou, *Adv. Energy Mater.* **2017**, 7(24), 1700278, <https://doi.org/10.1002/aenm.201700278>.
- [11] M. Armand, *Solid State Ion.* **1983**, 9–10, 745–754, [https://doi.org/10.1016/0167-2738\(83\)90083-8](https://doi.org/10.1016/0167-2738(83)90083-8).
- [12] X. Li, Q. Hou, W. Huang, H.-S. Xu, X. Wang, W. Yu, R. Li, K. Zhang, L. Wang, Z. Chen, K. Xie, K. P. Loh, *ACS Energy Lett.* **2020**, 5(11), 3498–3506, <https://doi.org/10.1021/acsenergylett.0c01889>.
- [13] L. R. Melby, R. J. Harder, W. R. Hertler, W. Mahler, R. E. Benson, W. E. Mochel, *J. Am. Chem. Soc.* **1962**, 84(17), 3374–3387, <https://doi.org/10.1021/ja00876a029>.

- [14] R. A. Heintz, H. Zhao, X. Ouyang, G. Grandinetti, J. Cowen, K. R. Dunbar, *Inorg. Chem.* **1999**, 38(1), 144–156, <https://doi.org/10.1021/ic9812095>.
- [15] F. Xu, S. Jin, H. Zhong, D. Wu, X. Yang, X. Chen, H. Wei, R. Fu, D. Jiang, *Sci. Rep.* **2015**, 5(1), 8225, <https://doi.org/10.1038/srep08225>.
- [16] B. Irié-Bi. Préparation et évaluation d'électrolyte solide organique à base de polymères organiques poreux pour l'assemblage de batterie tout solide tout organique. PhD Thesis (French), University of Picardie Jules Verne, Amiens, France, **2023**.
- [17] A. P. Côté, A. I. Benin, N. W. Ockwig, M. O'Keeffe, A. J. Matzger, O. M. Yaghi, *Science* **2005**, 310(5751), 1166–1170, <https://doi.org/10.1126/science.1120411>.
- [18] R. Precht, R. Hausbrand, W. Jaegermann, *Phys. Chem. Chem. Phys.* **2015**, 17(9), 6588–6596, <https://doi.org/10.1039/C4CP05206D>.
- [19] S. Wenzel, T. Leichtweiss, D. Krüger, J. Sann, J. Janek, *Solid State Ion.* **2015**, 278, 98–105, <https://doi.org/10.1016/j.ssi.2015.06.001>.
- [20] B. Irié-Bi; M. Becuwe, (third); F. Dolhem, (second). Novel All-Solid-State Electrolytes Based on Organoboron Covalent Organic Networks. Patent WO/2024/100209, Publication date 16.05.2024, <https://patentscope.wipo.int/search/en/detail.jsf?docId=WO2024100209>.
- [21] C. C. Liang, *J. Electrochem. Soc.* **1973**, 120(10), 1289, <https://doi.org/10.1149/1.2403248>.
- [22] F. W. Poulsen, N. H. Andersen, B. Kindl, J. Schoonman, *Solid State Ion.* **1983**, 9–10, 119–122, [https://doi.org/10.1016/0167-2738\(83\)90219-9](https://doi.org/10.1016/0167-2738(83)90219-9).
- [23] S. Pack, B. Owens, J. B. Wagner, *J. Electrochem. Soc.* **1980**, 127(10), 2177, <https://doi.org/10.1149/1.2129368>.
- [24] J. Maier, *Prog. Solid State Chem.* **1995**, 23(3), 171–263, [https://doi.org/10.1016/0079-6786\(95\)00004-E](https://doi.org/10.1016/0079-6786(95)00004-E).
- [25] H. Maekawa, Y. Fujimaki, H. Shen, J. Kawamura, T. Yamamura, *Solid State Ion. 15 Proc. 15th Int. Conf. Solid State Ion. Part II* **2006**, 177(26), 2711–2714, <https://doi.org/10.1016/j.ssi.2006.02.002>.
- [26] X. Judez, G. G. Eshetu, I. Gracia, P. López-Aranguren, J. A. González-Marcos, M. Armand, L. M. Rodríguez-Martínez, H. Zhang, C. Li, *ChemElectroChem* **2019**, 6(2), 326–330, <https://doi.org/10.1002/celec.201801390>.
- [27] T. M. W. J. Bandara, D. G. N. Karunathilaka, J. L. Ratnasekera, L. Ajith De Silva, A. C. Herath, B. E. Mellander, *Ionics* **2017**, 23(7), 1711–1719, <https://doi.org/10.1007/s11581-017-2016-y>.
- [28] B. Jinisha, K. M. Anilkumar, M. Manoj, A. Abhilash, V. S. Pradeep, S. Jayalekshmi, *Ionics* **2018**, 24(6), 1675–1683, <https://doi.org/10.1007/s11581-017-2332-2>.
- [29] G. G. Eshetu, X. Judez, C. Li, M. Martínez-Ibañez, I. Gracia, O. Bondarchuk, J. Carrasco, L. M. Rodríguez-Martínez, H. Zhang, M. Armand, *J. Am. Chem. Soc.* **2018**, 140(31), 9921–9933, <https://doi.org/10.1021/jacs.8b04612>.
- [30] S. S. Salehan, B. N. Nadirah, M. S. M. Saheed, W. Z. N. Yahya, M. F. Shukur, *J. Polym. Res.* **2021**, 28(6), 222, <https://doi.org/10.1007/s10965-021-02586-y>.
- [31] H. S. Lee, X. Q. Yang, C. L. Xiang, J. McBreen, L. S. Choi, *J. Electrochem. Soc.* **1998**, 145(8), 2813–2818, <https://doi.org/10.1149/1.1838719>.
- [32] B. Ma, L. Zhong, S. Huang, M. Xiao, S. Wang, D. Han, Y. Meng, *Molecules* **2024**, 29(8), 1759, <https://doi.org/10.3390/molecules29081759>.
- [33] J. Guo, F. Feng, X. Jiang, R. Wang, D. Chu, Y. Ren, F. Chen, P. He, Z.-F. Ma, S. Chen, T. Liu, *Adv. Funct. Mater.* **2024**, 34(26), 2313496, <https://doi.org/10.1002/adfm.202313496>.
- [34] R. Precht, S. Stolz, E. Mankel, T. Mayer, W. Jaegermann, R. Hausbrand, *Phys. Chem. Chem. Phys.* **2016**, 18(4), 3056–3064, <https://doi.org/10.1039/C5CP06659J>.
- [35] J. S. Miller, J. H. Zhang, W. M. Reiff, D. A. Dixon, L. D. Preston, A. H. Reis, E. Gebert, M. Extine, J. Troup, et al., *J. Phys. Chem.* **1987**, 91(16), 4344–4360, <https://doi.org/10.1021/j100300a028>.

Manuscript received: May 31, 2024  
Revised manuscript received: October 7, 2024  
Accepted manuscript online: October 7, 2024  
Version of record online: November 7, 2024